Vibrationally Induced Proton Transfer in $F^-(H_2O)$ and $F^-(D_2O)$

Samantha Horvath and Anne B. McCoy*

Department of Chemistry, The Ohio State University, Columbus, Ohio 43210

Joseph R. Roscioli and Mark A. Johnson*

Sterling Chemistry Laboratory, Yale University, P.O. Box 208107, New Haven, Connecticut 06520

Received: June 25, 2008; Revised Manuscript Received: September 23, 2008

Vibrational predissociation spectra of the $F^-(H_2O)\cdot Ar$ and $F^-(D_2O)\cdot Ar$ complexes are observed over a range of 600 to 3800 cm^{-1}, which include bands attributed to the fundamentals as well as the first two overtones of the vibrations primarily associated with the shared hydrogen. This information allows us to characterize both the extended potential surface confining the anionic H-bonded hydrogen and the degree to which this motion is coupled to the motions of other atoms in the complex. We analyze these new data with reduced dimensional treatments using explicit potential energy and electric dipole moment surfaces. The often employed one-dimensional treatment with fixed OF distance does not even qualitatively account for the observed isotope dependent level structures, but a simple extension to two dimensions, corresponding to the OF distance and the shared proton position, accurately recovers the observed spectra. The resulting two-dimensional wave functions are used to evaluate the extent of proton transfer in each vibrational level. The main conclusion of this work is that vibrational excitation of the shared proton can be regarded as optically driven, intracluster proton transfer.

I. Introduction

Ion−water complexes have become the topic of numerous spectroscopic studies covering both the intramolecular OH stretching region and, more recently, the lower frequency region that involves fundamental and overtone bands of the ion−molecule vibrational modes. Even within the simple class of the halide monohydrates, which all adopt asymmetric minimum energy structures involving ion attachment with a single hydrogen bond, a wide range of behavior is displayed according to the proton affinity (PA) of the anions. Large ions with relatively low PA, like iodide for example, can be treated in a perturbative limit. For these systems, a cut through the potential along the hydrogen bonded OH bond length (OH_b) appears very "Morse-like", and the OH_b stretching fundamental is redshifted from that of isolated H_2O by several hundred cm^{-1}.[1,2] In such cases, one expects that a one-dimensional model in which the OH_b vibration is uncoupled from the other degrees of freedom will be adequate. However as the PA of the anion approaches that of OH^-, the complexes become prototypical examples of short, strong hydrogen bonding and exhibit a number of interesting features.[2−11] In general, the potential energy curve associated with the motion of the light hydrogen atom parallel to the heavy atom axis becomes flattened relative to the typical quadratic shape. This allows for large amplitude motion of the shared proton even at the vibrational zero-point level[2,6] and is manifested in very low OH_b vibrational frequencies (typically <2000 cm^{-1}). In the limit of $OH^-(H_2O)$, for example, even though the potential that describes the displacement of the shared proton displays a small barrier, the zero point averaged ground state structures have the most probable position of the shared hydrogen equidistant between the heavy atoms.[12] In this case, shared proton motion away from the center of mass of the complex is strongly coupled to other low-frequency vibrations, in particular the OO stretch as well as the wags and rocks of the flanking OH groups. A similar coupling between the shared proton and heavy atom stretching motions has been reported by Del Bene and Jordan, based on their studies of $XH{:}NH_3$ (X = F, Cl, and Br) complexes.[13] For these reasons a one-dimensional picture cannot correctly capture the essential spectroscopic patterns displayed by these species.[10,14]

In this paper, we explore the coupled nature of the heavy atoms with that of the shared proton within a two-dimensional model of the $F^-(H_2O)$ in which displacements of the heavy atom bond (R_{OF}) and the OH_b bond (r_{OH_b}) are treated explicitly. The study addresses the extended level structure that is revealed by new measurements of the fundamental and overtone bands of the shared proton-based vibrations in $F^-(H_2O)$ and $F^-(D_2O)$ and the first overtone band of $F^-(HOD)$.

II. Overview of Previous Work on the $F^-(H_2O)$ Complex

We focus on the $F^-(H_2O)$ complex because it represents an interesting intermediate case of ionic hydrogen bonding, where different charge delocalization regimes are accessed by the first few vibrational levels of the shared proton stretch. The inset in Figure 1 shows its minimum energy structure, calculated at the MP2/aug-cc-pVTZ level of theory and basis. The complex forms a nearly linear $O-H_b\cdots F^-$ hydrogen bond, such that the OH_b bond length is extended by 0.106 Å relative to that in bare H_2O (0.961 Å). The length of the other OH bond is only 0.001 Å shorter than that in the bare species, and this second, free OH bond will be designated as OH_f in the discussion that follows.

Figure 1 also includes the one-dimensional cut through the potential surface, plotted as a function of the shared proton displacement from the center of the OF bond, with the OH_f distance and H_2O angle allowed to vary so as to minimize the energy of the system. The remaining three vibrational degrees

* Corresponding authors. E-mail: mccoy@chemistry.ohio-state.edu and mark.johnson@yale.edu.

10.1021/jp805616m CCC: $40.75
Published on Web 11/08/2008

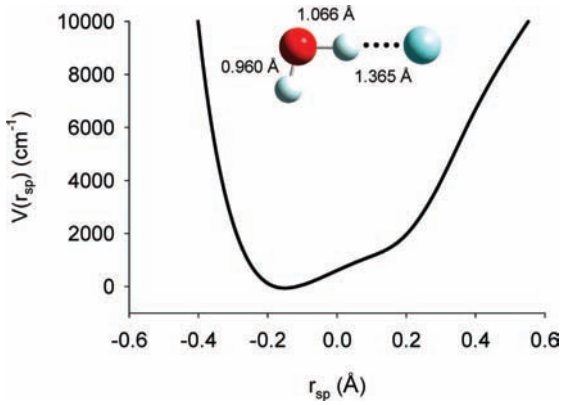

Figure 1. The one-dimensional potential, calculated at the MP2/aug-cc-pVTZ level of theory/basis, is plotted as a function of $r_{sp} = r_{OH_b} - {}^1/_2 R_{OF}$, which is approximately the displacement of the shared proton from the center of the OF bond. The minimum energy structure of the $F^-(H_2O)$ complex is also shown.

of freedom are constrained to their equilibrium values. Similar potentials have been calculated by several other groups,[9,15] and the overall qualitative picture is independent of the level of theory/basis. An important feature of this potential is the characteristic "shelf" structure near $r_{sp} \approx +0.1$ Å that results from the relatively low-lying energy of the $HO^- \cdots HF$ intracluster proton transfer configuration.

Schaefer and co-workers[15] were the first to treat the level structure expected for the shared proton in $F^-(H_2O)$. They employed a one-dimensional approximation using the calculated potential curve at the CISD/TZ2P+diff level of theory/basis, with the OF distance frozen at the equilibrium geometry and the shared proton confined to the heavy atom axis. Interestingly, subsequent measurement of the first overtone transition at 2905(20) cm^{-1} is in very good agreement with their predicted value of 2968 cm^{-1}.[16] Extension of the experimental coverage to the fundamental region was not accomplished until several years later,[2] and the observed 1523 cm^{-1} value was significantly below the 1667 cm^{-1} energy predicted for the fundamental transition on the same potential surface. Kim and co-workers[9] refined the one-dimensional approach (again at fixed OF distance) with a calculation at the CCSD(T)/TZ(2df,2pd)++ level of theory/basis and obtained fundamental (1481 cm^{-1}) and overtone energies (2951 cm^{-1}) in better agreement with experiment. More recently, Gerber and co-workers[8] used their CC-VSCF method to obtain fully coupled vibrational frequencies of the fundamental and first overtone of the shared proton stretch at the CCSD(T)/aug-cc-pVTZ level of theory/basis. They obtained frequencies of 1488 and 2888 cm^{-1},[8] respectively, which are close to those obtained from the one-dimensional study of Kim and co-workers[9] and still underestimate the fundamental transition.

In considering the qualitative features of the level structure, it is interesting to note that, after accounting for zero-point energy, the energy of the first excited state is anticipated to be on the order of 2400 cm^{-1}. This energy is sufficient to sample the shelf region of the potential plotted in Figure 1. In spite of the fact that this level accesses very anharmonic regions of the potential, all three calculations described above recover a frequency for the first overtone that is roughly twice that of the fundamental.

In this paper, we further explore the nature of the shared proton motion in a combined theoretical and experimental study of the $F^-(H_2O)$ system, where we extend earlier work on the $F^-(H_2O)$ vibrational structure to include states with up to three quanta in the OH_b (OD_b) stretch in both the $F^-(H_2O)$ and $F^-(D_2O)$ isotopologues as well as the state with two OH_b quanta in $F^-(HOD)$. Inclusion of these additional transitions and mass combinations allows us to more quantitatively determine how accurately the level structure can be accommodated within a one-dimensional picture.

From a theoretical standpoint, systems as small as these can be treated effectively with multidimensional anharmonic methods,[4,8,14,17−20] but it is often nontrivial to extract simple physical pictures from the final results. Here we take a more intuitive approach where we revisit the one-dimensional treatment described above, and then expand this analytical treatment to include a two-dimensional picture, where we elucidate how the shared proton vibration is coupled to the heavy atom stretch. In our two-dimensional calculations, we develop both potential energy and dipole moment surfaces, which extend over the range of the OH_b and OF distance coordinates that are explored by the lowest three or four vibrational levels involving excitation in the OH_b stretch. The resulting eigenstates are then combined with the calculated dipole moment surface to yield predicted band intensities, which can then be compared to the observed spectra. This analysis indicates that the one-dimensional model qualitatively fails to recover the observed isotope-dependence of the level structure, and agreement is substantially improved with the two-dimensional treatment.

III. Experimental Details

Argon-solvated cluster anions were generated by electron impact ionization (1 keV) of a pulsed free jet supersonic expansion and mass-selected in a tandem time-of-flight photofragmentation spectrometer described in detail previously.[21,22] The $F^-(H_2O)\cdot Ar$ complexes were synthesized using an entrainment approach, where trace amounts of NF_3 and H_2O vapor were introduced just outside the nozzle with independently controlled pulsed valves.[23]

Infrared spectra were recorded via argon predissociation spectroscopy:[24,25]

$$X^-(H_2O)\cdot Ar_n + h\nu \rightarrow X^-(H_2O)\cdot Ar_m + (n-m)Ar \quad (1)$$

where the argon-solvated anionic clusters were photoexcited with infrared pulses (600−3800 cm^{-1}, ~3 cm^{-1} resolution, with an accuracy of ±4 cm^{-1}) generated by a 10 Hz Nd:YAG pumped, KTP/KTA/$AgGaSe_2$-based OPO/OPA laser (Laser Vision). The spectra result from the addition of 10−20 individual scans and were normalized for variations in laser pulse energy over the spectral range. The entire path of the infrared laser beam up to the vacuum chamber was thoroughly purged with dry air to ensure minimal variation of laser power due to absorption of ambient water vapor, and the beam was introduced into the chamber through a KBr window.

IV. Theoretical Details

The approach used to characterize the $F^-(H_2O)$ complexes is based on both ab initio electronic structure and vibrational energy determinations. Ab initio calculations, performed using the Gaussian 03 software package,[26] were used to obtain one- and two-dimensional potential energy surfaces (PESs) and dipole moment surfaces (DMSs) as functions of r_{OH_b} (1-d) or r_{OH_b} and R_{OF} (2-d). These surfaces were calculated using second-order Möller-Plesset perturbation theory (MP2) with aug-cc-pVTZ Dunning basis sets, a combination of theory and basis set that has been reliable for halide−water systems.[27,28]

Three sets of potential energy and dipole moment surfaces are explicitly considered, which will be described as 1-d unrelaxed, 1-d relaxed, or 2-d in the presentation below. The calculated DMSs were shifted to have their origins at the center of mass and were rotated into an Eckart frame.[29,30] After rotation, the *a*-axis lies along the heavy atom axis, the *b*-axis is perpendicular to *a*, and these two axes define the plane of the molecule. The PESs and resulting DMSs were then used to calculate vibrational energies, wave functions, and transition moments in a potential optimized discrete variable representation (PO-DVR).[31−33]

To construct the one-dimensional unrelaxed PES, the electronic energy was calculated as a function of r_{OH_b} over a range of 0.3 to 1.8 Å in increments of 0.1 Å with $R_{OF} = R_{OF,e} =$ 2.43112 Å. For this potential energy slice, the remaining OH bond length (r_{OH_f}) and the water angle (θ_{HOH}) were allowed to relax, while all other internal coordinates were fixed at their equilibrium values. The one-dimensional DMS for the unrelaxed study was calculated over the same range of r_{OH_b}.

For the one-dimensional relaxed surface, the electronic energy was also calculated as a function of the r_{OH_b} distance, which ranged from 0.5 to 5.9 Å in increments of 0.05 Å. The internal coordinates related to the water molecule, r_{OH_f} and θ_{HOH}, were relaxed as for the above one-dimensional surface. However, the important difference between these two, one-dimensional PESs is that the heavy atom distance, R_{OF}, is allowed to relax at every value of r_{OH_b}. The remaining two geometric parameters were held constant at their respective equilibrium values. The one-dimensional relaxed DMS was calculated on a smaller grid than its corresponding PES, 0.60 to 2.50 Å in increments of 0.05 Å. For the calculations of the PESs and DMSs presented above, the planarity of the complex was retained.

Finally for the two-dimensional surface, the electronic energy was calculated over a range from 1.83112 to 3.43112 Å in R_{OF} and 0.56680 to 3.15680 Å in r_{OH_b}, both in increments of 0.01 Å. For these calculations, the four atoms were constrained to remain planar, and the H_fOF angle was fixed at its equilibrium value of 100.61816°. All other internal coordinates were allowed to relax. The two-dimensional DMS was calculated over a range from 2.03112 to 3.03112 Å in R_{OF} and 0.66680 to 1.76680 Å in r_{OH_b} in increments of 0.1 Å. The ranges for all one- and two-dimensional PESs and DMSs were chosen such that they spanned the region of the potential that is sampled by the vibrational wave functions of the states with up to three quanta of excitation in the OH_b stretch.

For the two, one-dimensional calculations, the Hamiltonian is given by

$$\hat{H} = -\frac{1}{2\mu_r}\frac{d^2}{dr^2} + V(r) \qquad (2)$$

where $\hbar = 1$ throughout this discussion. In eq 2, $V(r)$ is obtained by using a cubic spline interpolation of the ab initio data points. For the relaxed one-dimensional surface, $r = r_{OH_b}$ at fixed R_{OF}, and the reduced mass is that associated with an OH stretch. For the calculations using the unrelaxed potential, $r = r_{OH_b} - {}^1/_2 R_{OF,e}$, or $r \approx {}^1/_2(r_{OH_b} - r_{HF})$. Here μ_r is the reduced mass associated with this motion when the angle between r_{OH_b} and r_{HF} is fixed at its equilibrium value of 177.53917°. For the 1-d relaxed and 1-d unrelaxed studies of the OH_b (OD_b) stretch, the reduced masses are 0.948087 (1.788848) amu and 0.979847 (1.904547) amu, respectively. For the relaxed PES, *r* varied from 0.45 to 6.5 Å with 550 grid points, while the unrelaxed PES ranged from −1.0 to 1.0 Å with 400 grid points.

The general two-dimensional stretch Hamiltonian, which incorporates both r_{OH_b} and R_{OF}, is given by

$$\hat{H} = -\frac{1}{2\mu_r}\frac{\partial^2}{\partial r_{OH_b}^2} - \frac{1}{2\mu_R}\frac{\partial^2}{\partial R_{OF}^2} - \frac{1}{2}\frac{\partial}{\partial r_{OH_b}}\frac{\cos\theta(r_{OH_b}, R_{OF})}{m_O}\frac{\partial}{\partial R_{OF}} - \frac{1}{2}\frac{\partial}{\partial R_{OF}}\frac{\cos\theta(r_{OH_b}, R_{OF})}{m_O}\frac{\partial}{\partial r_{OH_b}} + V(r_{OH_b}, R_{OF}) \qquad (3)$$

where μ_i ($i = r$ or R) is the reduced mass associated with each stretch coordinate, 0.948087 (1.788848) and 8.683882 amu for the OH_b (OD_b) and OF bonds, respectively, and m_O is the mass of oxygen. In the mixed partial derivatives $\theta(r_{OH_b},R_{OF})$ is the H_bOF angle and has an equilibrium value of 1.38125°. A bicubic spline interpolation of the ab initio points was used to calculate $\theta(r_{OH_b},R_{OF})$ at every value of r_{OH_b} and R_{OF} on the two-dimensional grid. The two-dimensional potential energy surface for the two stretch coordinates, $V(r_{OH_b},R_{OF})$, was similarly acquired. To solve eq 3, we used a PO-DVR in each of the two stretch coordinates. These potentials were obtained by fitting a slice through the two-dimensional PES at the equilibrium value of the other coordinate ($R_{OF} = 2.43112$ Å or $r_{OH_b} = 1.06680$ Å) to a fifth-order Taylor series expansion in the OF bond displacement coordinate and an eighth-order expansion in the displacement of r_{OH_b}. The one-dimensional Schrödinger equations were each solved in a harmonic oscillator basis using 400 functions. The eigenfunctions were then transformed to generate a DVR with 50 points, and the matrix representations of the momenta conjugate to r_{OH_b} and R_{OF} were evaluated in this representation. The two-dimensional stretch Hamiltonian was solved in the product basis, using the 50 DVR points in both r_{OH_b} and R_{OF}.

The wave functions were then used to evaluate the vibrationally averaged rotational constants, which were used to obtain the rotational energies for each vibrational state and line strengths of the transitions. As such the rotational and vibrational stick spectra were convoluted together with a Gaussian with a half-width half-maximum (hwhm) of 1 cm^{-1}. These spectra were calculated over a range of vibrational temperatures (50−100 K). As the temperature dependence of the spectra is small, only the results for 50 K will be reported.

V. Results and Discussion

V.A. Appearance and Isotope Dependence of the Ar-Tagged $F^-(H_2O)$ Spectra. Figure 2 presents the Ar-predissociation spectra of the $F^-(H_2O)$ and $F^-(D_2O)$ complexes in traces 2(a) and 2(b), respectively. The OH and OD stretching fundamentals are very intense features because of the low-lying $HO^-\cdots HF$ configuration, which allows for significant charge transfer upon vibrational excitation.[2] This anharmonicity lends itself to the observation of overtones in the OH_b stretch, and these (albeit weaker) transitions are labeled in Figure 2 by $\nu_{IHB}^{n\leftarrow 0}$, where *n* represents the number of quanta in the intramolecular hydrogen bond (IHB) after vibrational excitation. Note that the IHB stretch bands all exhibit significant multiplet structure, the origin of which is not yet understood. We have found these band profiles to be dependent upon the number of Ar atoms attached to the cluster, and future studies are therefore aimed at obtaining the infrared spectra of Ne-tagged or bare ion complexes to determine the role of Ar in the band profiles.

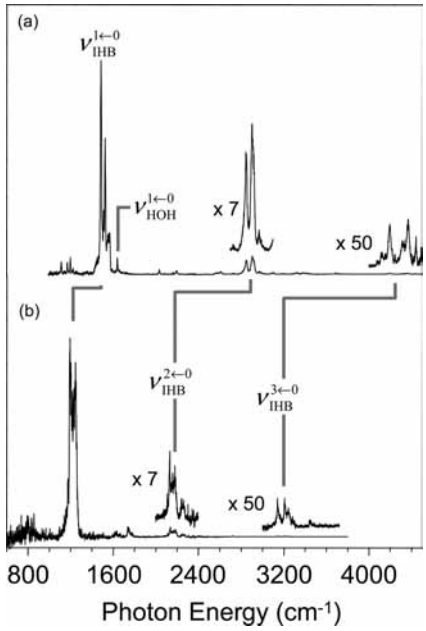

Figure 2. Ar-predissociation spectra of (a) $F^-(H_2O)$ and (b) $F^-(D_2O)$.

TABLE 1: Comparison of Various Calculated Anharmonic Frequencies with Experiment[a]

	1-d unrelaxed	1-d relaxed	2-d	expt[b]
$F^-(H_2O)$				
$\nu_{IHB}^{1\leftarrow0}$	1497 (1.1888)	1405 (1.3757)	1533 (1.0000)	1430−1570
$\nu_{IHB}^{2\leftarrow0}$	3159 (0.0204)	2649 (0.1366)	2934 (0.0216)	2815−2930
$\nu_{IHB}^{3\leftarrow0}$	5009 (0.0009)	3810 (0.0171)	4469 (0.0007)	4110−4450
$F^-(D_2O)$				
$\nu_{IHB}^{1\leftarrow0}$	1089 (0.8326)	1084 (1.0690)	1166 (0.5479)	1160−1270
$\nu_{IHB}^{2\leftarrow0}$	2177 (0.0223)	2035 (0.0848)	2142 (0.0238)	2120−2263
$\nu_{IHB}^{3\leftarrow0}$	3421 (0.0010)	2929 (0.0080)	3230 (0.0013)	3125−3265

[a] All frequencies are given in cm^{-1}, and the relative values of M_n [defined in eq 5] are listed in parentheses. [b] $F^-(HOD)$: $\nu_{IHB}^{2\leftarrow0}$ range 2800−2930.

We also point out several other experimentally observed transitions. First, the HOH bend, ($\nu_{HOH}^{1\leftarrow0}$ in Figure 2a) appears just above the strong IHB fundamental at 1638 cm^{-1}, near the bend frequency of a free water molecule (1595 cm^{-1}).[34] This implies that the fluoride-bound water molecule is largely intact at the zero-point level. However, upon excitation to the state with one quantum in the OH_b stretch, we would expect its frequency to dramatically change due to the charge transfer nature of the IHB transition. The DOD bend should be red-shifted from that of the HOH by roughly the ratio of the bend frequencies of isolated DOD and HOH (0.739), but this estimated value of 1210 cm^{-1} falls in the center of the OD_b ν_{IHB} fundamental. Interestingly, despite the fact that the OD_b stretch and the bend are nearly degenerate, they do not appear to mix significantly; in fact, the shared OD $\nu_{IHB}^{1\leftarrow0}$ band is actually *less* structured than its OH counterpart. This experimental observation is supported by the normal mode picture, in which little coupling is observed between the OD stretch and the DOD bend at the harmonic level.

In what follows we will focus on the coupling between the shared proton and OF stretching vibrations as the key to understanding the level structure, and one way to empirically investigate the role of the dangling OH_f is to determine how the energies of the OH_b stretch levels respond to H/D substitution at this site. We therefore also studied the $F^-(HOD)$ complex. Because the lighter H fractionates very efficiently to the shared position,[1] we were only able to compare the shared proton vibrations for the $F^-(H_2O)$ and $F^-(HOD)$ variations, with the results presented as a footnote in Table 1. The IHB bands are quite similar in these two molecules, indicating that the motions of the dangling hydrogen atoms are not intimately coupled to the shared proton band positions.

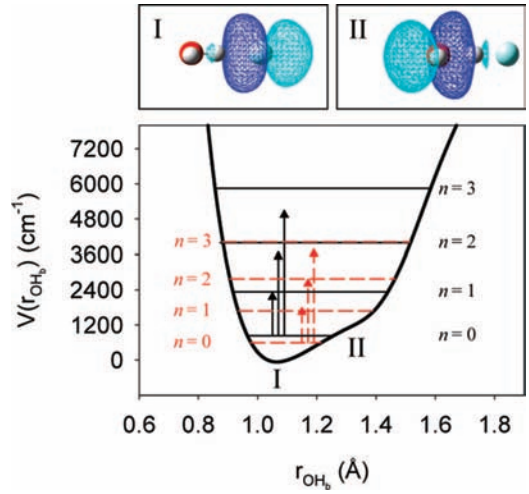

Figure 3. The 1-d unrelaxed PES with black and red horizontal lines indicating the calculated energies of the OH_b and OD_b stretches, respectively. The black and red arrows provide the center of the experimental ranges reported in Table 1. Natural bond orbitals for the excess electron are shown above.

V.B. Investigation of OH_b Frequency Progressions. To characterize the shared proton potential, it is useful to first consider what the experimental frequencies tell us about the potential surface. It has long been recognized that the progression of vibrational levels of an XH oscillator can be well described by a Morse potential for which

$$\tilde{\nu}_n = \tilde{\nu}_e n - \tilde{\nu}_e \chi_e (n^2 + n) \quad (4)$$

To obtain fundamental and anharmonicity constants, we fit the center of intensity for each observed band to eq 4. On the basis of this analysis, we find that the ratio of the anharmonicity to the frequency is roughly 0.02 for the OH_b stretch and approximately 0.04 for the OD_b stretch. While it is surprising to find an OD stretch that is more anharmonic than an OH stretch, the ratios are not significantly larger than what one would obtain for bare H_2O or D_2O for which the ratios are both approximately 0.01.[35]

This relatively small anharmonicity was not foreseeable given the large (>2000 cm^{-1}) redshift in the OH_b fundamental transition relative to the free OH stretch at ~3690 cm^{-1}.[2] Clearly a single one-dimensional Morse oscillator will not reproduce the observed isotope-dependent level structure. To explore the connection of the spectral features to the underlying potential surface, we start with the same approach that has been used in a number of earlier studies[9,15] on this system and examine the one-dimensional PESs and their resulting frequencies.

V.C. Examination of Transition Energies from the 1-d PESs. The one-dimensional, unrelaxed potential energy surface is shown as the thick, black curve in Figure 3. An important feature of this surface is the presence of the shelf structure, which arises from an avoided crossing between the two diabatic potentials that correspond to the $F^-\cdots H_2O$ and $HO^-\cdots HF$ complexes. These two configurations are illustrated by the natural bond orbitals (NBOs) for the excess electron[36−38] shown

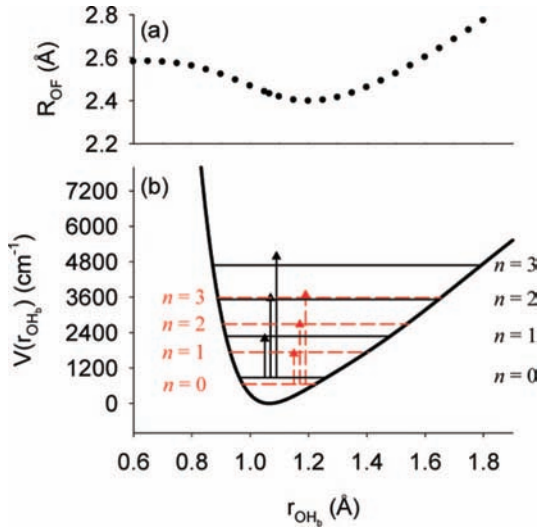

Figure 4. The lower panel (b) is the same as that shown in Figure 3, but with the 1-d relaxed PES, as described in the text. In panel a, we plot the OF internuclear distance as a function of the OH_b bond length, plotted on the same scale as panel b.

at the top of Figure 3. The NBO in Figure 3 orbital I is localized on the fluoride; however, the other NBO, in Figure 3 orbital II, is localized on the oxygen. Thus for $r_{OH_b} < 1.286$ Å, the excess electron can be considered to be localized on the F atom, while for longer OH_b distances, the excess electron has migrated from F to O. This value of r_{OH_b} coincides with the shelf region of the potential plotted in Figure 3.

As described above, the vibrational levels for the shared proton motion, based on this potential, were obtained by numerically solving the Schrödinger equation based on the Hamiltonian given in eq 2. These results are reported in Table 1 and are represented by red and black horizontal lines in Figure 3. As noted in the Introduction, the state with one quantum of excitation in the OH_b stretch lies above the shelf region. As such we expect it to exhibit some $HO^-\cdots HF$ character.

To aid in the comparison between the experimental and calculated frequencies, the experimental transition energies are depicted by the black and red vertical arrows for the OH and OD stretches, respectively, with their origins placed at the calculated zero-point levels. Like the previous one-dimensional treatments,[15] this PES reproduces the fundamental and first overtone frequencies for the OH stretch in $F^-(H_2O)$, and in addition yields reasonable values for the fundamental and first overtone transitions of the OD stretch in $F^-(D_2O)$ as well. There is, however, poor agreement for the second overtone frequency of both the OH and OD stretches as shown in Table 1. No single, multiplicative scaling of the potential can correct for this discrepancy.

To further investigate these systems, we now turn our attention to the one-dimensional, relaxed PES shown in Figure 4. Note that this treatment is analogous to an adiabatic adjustment of the OF distance along the shared proton stretch coordinate, providing a contrasting scenario to the situation presented in Figure 3, where there was no coupling between these motions. By allowing R_{OF} to change, the shelf structure is lost entirely, making the effects of proton transfer less visible. Here the fundamental frequencies for the both OH stretch in $F^-(H_2O)$ and the OD stretch in $F^-(D_2O)$ agree well with experiment. However, the energies of the first and second overtones in the OH and OD stretches are now too low, and again no single, multiplicative scaling of the PES will correct this.

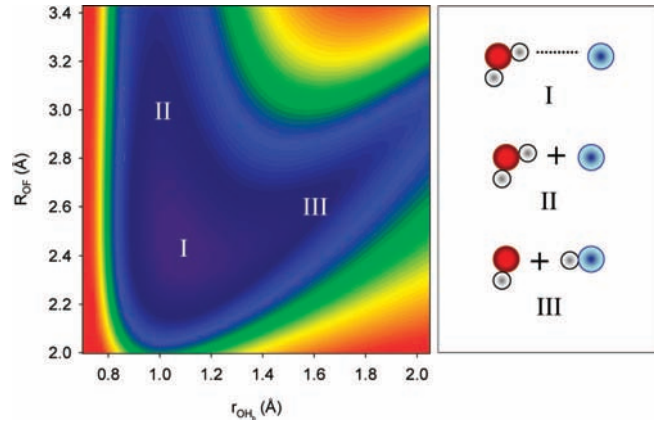

Figure 5. The two-dimensional potential for $F^-\cdots H_2O$. Complex I is the minimum energy structure, $F^-\cdots H_2O$. Complex II shows the dissociation of the minimum energy structure into $H_2O + F^-$ upon excitation in R_{OF}. Complex III shows the dissociation of the minimum energy structure into $HO^- + HF$ upon excitation in both R_{OF} and r_{OH_b}.

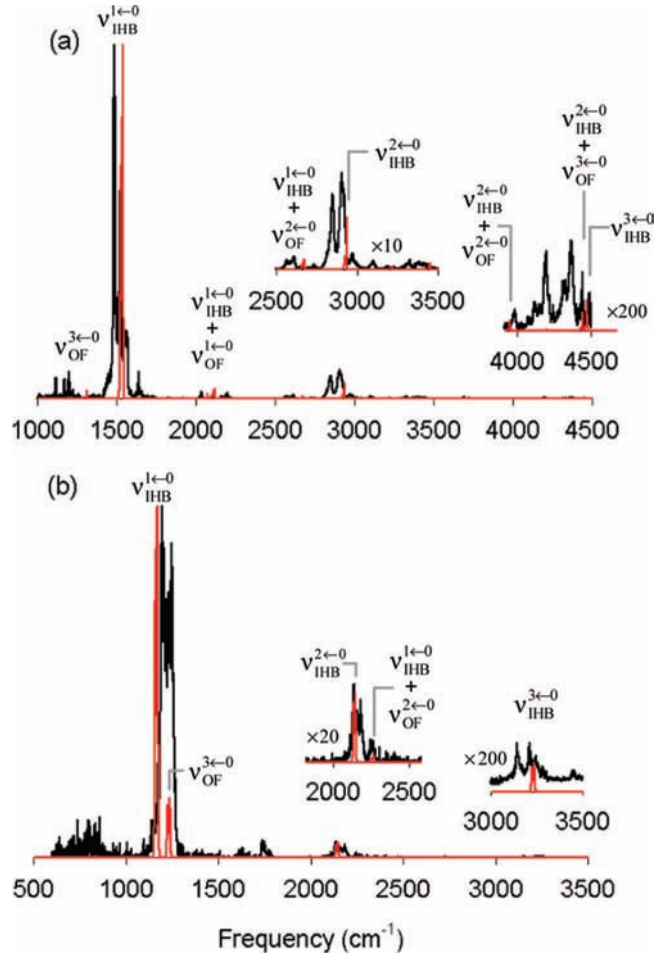

Figure 6. Comparison of the convoluted stick spectra with experiment for (a) $F^-(H_2O)$ and (b) $F^-(D_2O)$. Each pair of spectra has been scaled so that they have the same value for the maximum peak height.

On the basis of these two limiting models, we find that the one-dimensional PESs each reproduce a portion of the experimental progression for $F^-(H_2O)$ and $F^-(D_2O)$, but all six transitions cannot simultaneously be reproduced with either one-dimensional picture. In considering how to fully describe the H^+ transfer dynamics in $F^-(H_2O)$, we note that there is strong coupling between R_{OF} and r_{OH_b} as shown in Figure 4a, with

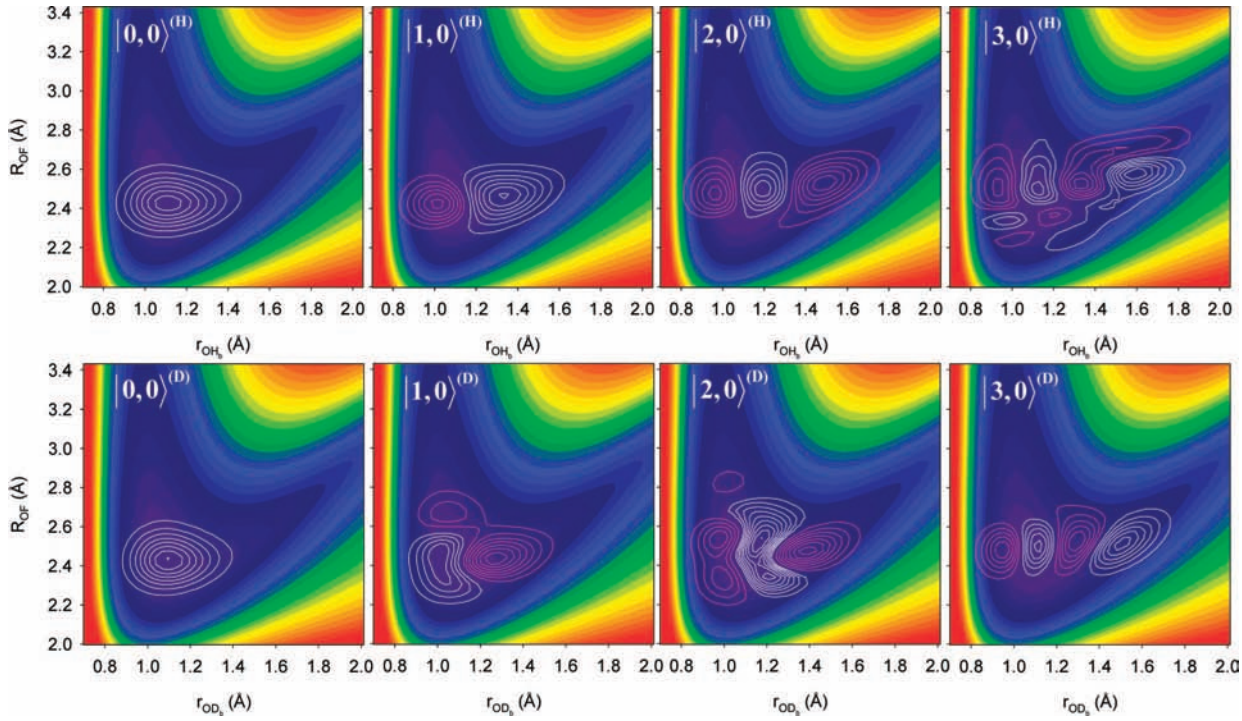

Figure 7. Two-dimensional wave functions for $F^-(H_2O)$ and $F^-(D_2O)$ are overlaid on the two-dimensional potential. The state labels provide the numbers of quanta in the OH_b and OF stretches, respectively.

TABLE 2: The Average Values of ρ_{PT}[a] and Percent Proton Transfer[b]

state	$\langle\rho_{PT}\rangle$/Å	% proton transfer
	$F^-(H_2O)$	
$n = 0$	−0.2236	14.95
$n = 1$	−0.0264	58.35
$n = 2$	0.0334	52.90
$n = 3$	0.0803	62.01
	$F^-(D_2O)$	
$n = 0$	−0.2550	8.99
$n = 1$	−0.1123	45.25
$n = 2$	−0.0530	50.48
$n = 3$	0.0037	53.32

[a] Defined in eq 6. [b] For $\rho_{PT} > 0$, the proton is associated with F rather than O.

large changes in R_{OF} over a relatively small range in r_{OH_b}, even near the equilibrium, $r_{OH_b} = 1.067$ Å.

V.D. Results from the 2-d Treatment. ***V.D.1. Comparison between Calculated and Experimental Transition Frequencies.*** The two-dimensional PES is plotted as a function of r_{OH_b} and R_{OF} in Figure 5. This potential can be divided into three regions, denoted by their corresponding structures. The minimum energy configuration, $F^-\cdots H_2O$, is indicated as structure I; at large values of R_{OF}, the complex dissociates into $F^- + H_2O$ (structure II), while at large values of both r_{OH_b} and R_{OF}, the complex dissociates into $HO^- + HF$ (structure III). We include the associated anharmonic transition frequencies in Table 1. Comparing the three sets of calculated values, we find that this model provides the best agreement with the experimental values for both isotopologues. To obtain this agreement, we multiplied all of the electronic energies used to construct the two-dimensional surface by 0.99, which is consistent with the scaling factors used for this level of theory and a comparable basis set.[39−41] This scaling led to a decrease in the transition frequencies by roughly 0.6% or between 9 and 33 cm^{-1}, and even without scaling, the calculated frequencies are in very good agreement with experimental values.

V.D.2. Comparison of Calculated Spectra with Experiment. Having demonstrated that the experimental frequency progressions are reproduced by the two-dimensional ab initio potential surface, we turn our attention to the calculated spectra, which we compare with experiment in Figure 6. The red curve is a convolution of the stick spectra calculated at a rotational temperature of 50 K and convoluted with a Gaussian with a hwhm of 1 cm^{-1}. The experimental spectra are shown as the black traces in Figure 6 and are identical to those shown in Figure 2.

In Table 1 we report the square of the transition moments for the OH_b or OD_b stretch,

$$M_n^{(H/D)} = \frac{|\langle n|\vec{\mu}|0\rangle|^2_{H/D}}{|\langle 1|\vec{\mu}|0\rangle|^2_{H}} \quad (5)$$

for the fundamental and first two overtone transitions. All of the reported transition moments have been normalized with respect to the fundamental transition of the OH_b stretch in $F^-(H_2O)$, $|\langle 1|\vec{\mu}|0\rangle|^2_H$, from the 2-d calculation. We have reported $M_n^{(H/D)}$ values rather than the usual intensities because the reported experimental signal reflects the measured signal divided by the laser power. This ratio is equivalent to dividing the calculated intensity by the transition frequency.

To begin, we will consider the $F^-(D_2O)$ spectrum shown in Figure 6b. The three OD_b stretch frequencies agree very well with experiment, and the relative peak heights are in qualitative agreement. Upon closer examination of the deuterated spectrum, there is additional structure near two of the three transitions. There is a strong feature that lies underneath the $\nu_{HB}^{1\leftarrow 0}$ experimental peak. This band occurs at 1232 cm^{-1} and is attributed to the $\nu_{OF}^{3\leftarrow 0}$ band. This feature might be leading to some of the extra structure seen in the $\nu_{HB}^{1\leftarrow 0}$ peak in the experimental spectrum. A second peak of interest lies to the blue of $\nu_{HB}^{2\leftarrow 0}$. This peak appears at 2263 cm^{-1} and is attributed to the $\nu_{HB}^{1\leftarrow 0} + \nu_{OF}^{2\leftarrow 0}$ combination band.

As with the $F^-(D_2O)$ spectrum, the calculated positions of the three main transitions in the $F^-(H_2O)$ spectrum agree well with experiment, but the relative peak heights are in less good agreement. In addition, bands in the experimental $F^-(H_2O)$ spectrum are even more structured than those in $F^-(D_2O)$. For example the $\nu_{IHB}^{2\leftarrow 0}$ band is clearly a doublet. Upon closer examination of the region near $\nu_{IHB}^{1\leftarrow 0}$, there is a second, much smaller peak that is close to our calculated $\nu_{OF}^{3\leftarrow 0}$ band at 1308 cm^{-1}. This transition is much weaker than the corresponding transition in $F^-(D_2O)$ because the $\nu_{OF}^{3\leftarrow 0}$ peak is separated from $\nu_{IHB}^{1\leftarrow 0}$ by ~225 cm^{-1}, whereas this difference is only ~65 cm^{-1} for the deuterated species. In the calculated spectrum, a second peak to the red of $\nu_{IHB}^{2\leftarrow 0}$ occurs at 2668 cm^{-1} and corresponds to the $\nu_{IHB}^{1\leftarrow 0} + \nu_{OF}^{2\leftarrow 0}$ combination band. This peak has comparable transition strength to that of $\nu_{IHB}^{3\leftarrow 0}$. Moreover there is a similarly spaced peak present in the experimental spectrum. As is evident by the experimental spectrum of $F^-(H_2O)$, $\nu_{IHB}^{3\leftarrow 0}$, like the other two transitions, has intriguing peak structure. There are two calculated features in this region at 3950 and 4439 cm^{-1} that are combination bands of $\nu_{IHB}^{2\leftarrow 0} + \nu_{OF}^{2\leftarrow 0}$ and $\nu_{IHB}^{2\leftarrow 0} + \nu_{OF}^{3\leftarrow 0}$, respectively. These two transitions have calculated integrated intensities that are nearly equal to that of the nearby $\nu_{IHB}^{3\leftarrow 0}$ transition.

Both the experimental and calculated $F^-(H_2O)$ spectra show additional structure in the region between 2000 and 2400 cm^{-1}. In the calculated spectrum, the feature at 2112 cm^{-1} results from a combination band of $\nu_{IHB}^{1\leftarrow 0} + \nu_{OF}^{1\leftarrow 0}$ and might correspond to the experimental feature near 2250 cm^{-1}. On the basis of our calculations, we find that this transition has similar transition strength as the first overtone in the OH_b stretch. As a final note, we suspect that the experimental feature near 2000 cm^{-1} is the overtone in the out-of-plane bend and is the subject of current investigation.[42]

Up to this point, we have focused on transitions with energies equal to or greater than 600 cm^{-1}, i.e., spectral regions where transitions can be measure experimentally. In addition to these transitions, we determine the $\nu_{OF}^{1\leftarrow 0}$ feature for both $F^-(H_2O)$ and $F^-(D_2O)$ to have frequencies and transition moments of 465 (0.2234) and 427 cm^{-1} (0.3051), respectively. The first overtones are predicted to occur at 898 and 833 cm^{-1}, respectively, and are anticipated to have comparable transition moments to that of $\nu_{IHB}^{3\leftarrow 0}$.

V.D.3. Quantifying the Vibrational Level Dependence of the Extent of Proton Transfer. We conclude our discussion of the fluoride−water complexes by focusing on other properties that can be derived by analysis of the wave functions. Paramount among these is understanding and quantifying the degree to which proton transfer is driven by vibrational excitation of the OH_b stretch. To do so we focus on the two-dimensional wave functions for $F^-(H_2O)$ and $F^-(D_2O)$, which are displayed in Figure 7 and plotted on top of the PES, where the white or pink striations denote the phase of the wave function. The state labels correspond to the numbers of quanta in r_{OH_b} and R_{OF}, respectively. Thus the plots labeled by $|0,0\rangle^{(H/D)}$ in Figure 7 are of the ground vibrational states of $F^-(H_2O)$ and $F^-(D_2O)$, respectively. The remaining six plots in Figure 7 have one, two, and three quanta of excitation in the OH stretch.

Examination of the excited state wave functions indicates that, when the OH_b bond is vibrationally excited, the wave function exhibits significant amplitude in the proton transfer region ($r_{OH_b} \gtrsim 1.286$ Å). To quantify the extent to which H^+ transfer is driven by vibrational excitation of the OH or OD stretch, we define[2,43,44]

$$\rho_{PT} = (r_{OH} - r_{OH}^0) - (r_{HF} - r_{HF}^0) \quad (6)$$

which is an index that allows us to quantify the degree of proton transfer in proton-bound complexes. In eq 6, r_{XH}^0 denotes the equilibrium OH or HF distance in a bare water or HF molecule, respectively. For the case of bare water, $r_{OH}^0 = 0.96148$ Å, and for HF, $r_{HF}^0 = 0.92183$ Å, for the structures calculated at the MP2/aug-cc-pVTZ level of theory/basis. With this definition, we can then determine what fraction of the probability amplitude can be characterized as $HO^-\cdots HF$ ($\rho_{PT} > 0$), which provides a measure of the percentage of proton transfer in each vibrational state. These percentages, along with $\langle\rho_{PT}\rangle$, are listed in Table 2. The percent of proton transfer in the ground state is 15% for $F^-(H_2O)$ and 9% for $F^-(D_2O)$. However, even one quantum in r_{OH_b} yields proton transfer of ~60% for $F^-(H_2O)$ and ~50% for $F^-(D_2O)$. Note that while there is a substantial increase in the percentages of proton transfer from the ground to first excited state, they remain nearly constant for the three excited states. While this observation many seem surprising, it reflects a buildup of probability amplitude above the shelf region of the potential in these excited states.

VI. Conclusion

Through H/D isotopic substitution and spectroscopic observation of the fundamental and first two overtone transitions associated with the shared proton, we obtain an extensive database from which to explore both the nature of the shared proton potential surface and the extent to which its motion is coupled to the motions of other atoms in the complex. Although one-dimensional treatments are common in the literature, we find that such a simple analysis cannot accurately recover either the higher overtones or the isotope dependence of the observed bands. We identify the OF stretch as the critical motion necessary to include for an accurate description of the observed levels. Explicit two-dimensional analysis of the vibrational levels and transition moments on an extended potential surface yields transitions quite close to the observed bands. This is a reflection of the effective OF distance being elongated at the higher levels of shared proton excitation. Analysis of the resulting wave functions indicates that while the zero-point level is largely charge localized on the fluoride ion, all the excited states associated with the shared proton stretch conform to situations where the bridging proton is largely equally shared. The large intensity of the infrared transitions can thus be traced to optically driven, intracluster proton transfer, as inferred in earlier reports of the spectrum.[16]

Acknowledgment. A.B.M. and M.A.J. would like to thank the chemistry division of the National Science Foundation for support of this work. We also thank the Ohio Supercomputer Center for an allocation of computing resources.

References and Notes

(1) Diken, E. G.; Shin, J.-W.; Price, E. A.; Johnson, M. A. *Chem. Phys. Lett.* **2004**, *387*, 17.

(2) Roscioli, J. R.; Diken, E. G.; Johnson, M. A.; Horvath, S.; McCoy, A. B. *J. Phys. Chem. A* **2006**, *110*, 4943.

(3) Roscioli, J. R.; McCunn, L. R.; Johnson, M. A. *Science* **2007**, *316*, 249.

(4) Hammer, N. I.; Diken, E. G.; Roscioli, J. R.; Johnson, M. A.; Myshakin, E. M.; Jordan, K. D.; McCoy, A. B.; Huang, X.; Bowman, J. M.; Carter, S. *J. Chem. Phys.* **2005**, *122*, 244301.

(5) Diken, E. G.; Headrick, J. M.; Roscioli, J. R.; Bopp, J. C.; Johnson, M. A.; McCoy, A. B.; Huang, X.; Carter, S.; Bowman, J. M. *J. Phys. Chem. A* **2005**, *109*, 571.

(6) Diken, E. G.; Headrick, J. M.; Roscioli, J. R.; Bopp, J. C.; Johnson, M. A.; McCoy, A. B. *J. Phys. Chem. A* **2005**, *109*, 1487.

(7) McCunn, L. R.; Roscioli, J. R.; Johnson, M. A.; McCoy, A. B. *J. Phys. Chem. B* **2008**, *112*, 321.

(8) Chaban, G. M.; Xantheas, S. S.; Gerber, R. B. *J. Phys. Chem. A* **2003**, *107*, 4952.

(9) Kim, J.; Lee, H. M.; Suh, S. B.; Majumdar, D.; Kim, K. S. *J. Chem. Phys.* **2000**, *113*, 5259.

(10) McCoy, A. B.; Huang, X.; Carter, S.; Bowman, J. M. *J. Chem. Phys.* **2005**, *123*, 064317.

(11) Taylor, M. S.; Muntean, F.; Lineberger, W. C.; McCoy, A. B. *J. Chem. Phys.* **2004**, *121*, 5688.

(12) Samson, C. C. M.; Klopper, W. *J. Mol. Struct. THEOCHEM* **2002**, *586*, 201.

(13) Del Bene, J. E.; Jordan, M. J. T. *J. Chem. Phys.* **1998**, *108*, 3205.

(14) McCoy, A. B.; Huang, X.; Carter, S.; Landeweer, M. Y.; Bowman, J. M. *J. Chem. Phys.* **2005**, *122*, 061101.

(15) Yates, B. F.; Schaefer, H. F.; Lee, T. J.; Rice, J. E. *J. Am. Chem. Soc.* **1988**, *110*, 6327.

(16) Ayotte, P.; Kelley, J. A.; Nielsen, S. B.; Johnson, M. A. *Chem. Phys. Lett.* **2000**, *316*, 455.

(17) Huang, X.; Cho, H. M.; Carter, S.; Ojamäe, L.; Bowman, J. M.; Singer, S. J. *J. Phys. Chem. A* **2003**, *107*, 7142.

(18) Huang, X. C.; Braams, B. J.; Carter, S.; Bowman, J. M. *J. Am. Chem. Soc.* **2004**, *126*, 5042.

(19) Chaban, G. M.; Jung, J. O.; Gerber, R. B. *J. Phys. Chem. A* **2000**, *104*, 2772.

(20) Vendrell, O.; Gatti, F.; Meyer, H.-D. *J. Chem. Phys.* **2007**, *127*, 184303.

(21) Posey, L. A.; DeLuca, M. J.; Johnson, M. A. *Chem. Phys. Lett.* **1986**, *131*, 170.

(22) Johnson, M. A.; Lineberger, W. C. Pulsed Methods for Cluster Ion Spectroscopy. In *Techniques for the Study of Ion−Molecule Reactions*; Farrar, J. M., Saunders, W. H., Jr., Eds.; Wiley: New York, 1988; Vol. XX, pp 591.

(23) Robertson, W. H.; Kelley, J. A.; Johnson, M. A. *Rev. Sci. Instrum.* **2000**, *71*, 4431.

(24) Okumura, M.; Yeh, L. I.; Myers, J. D.; Lee, Y. T. *J. Chem. Phys.* **1986**, *85*, 2328.

(25) Ayotte, P.; Weddle, G. H.; Kim, J.; Johnson, M. A. *Chem. Phys.* **1998**, *239*, 485.

(26) Frisch, M. J.; Trucks, G. W.; Schlegel, H. B.; Scuseria, G. E.; Robb, M. A.; Cheeseman, J. R.; Montgomery, J. A., Jr.; Vreven, T.; Kudin, K. N.; Burant, J. C.; Millam, J. M.; Iyengar, S. S.; Tomasi, J.; Barone, V.; Mennucci, B.; Cossi, M.; Scalmani, G.; Rega, N.; Petersson, G. A.; Nakatsuji, H.; Hada, M.; Ehara, M.; Toyota, K.; Fukuda, R.; Hasegawa, J.; Ishida, M.; Nakajima, T.; Honda, Y.; Kitao, O.; Nakai, H.; Klene, M.; Li, X.; Knox, J. E.; Hratchian, H. P.; Cross, J. B.; Bakken, V.; Adamo, C.; Jaramillo, J.; Gomperts, R.; Stratmann, R. E.; Yazyev, O.; Austin, A. J.; Cammi, R.; Pomelli, C.; Ochterski, J. W.; Ayala, P. Y.; Morokuma, K.; Voth, G. A.; Salvador, P.; Dannenberg, J. J.; Zakrzewski, V. G.; Dapprich, S.; Daniels, A. D.; Strain, M. C.; Farkas, O.; Malick, D. K.; Rabuck, A. D.; Raghavachari, K.; Foresman, J. B.; Ortiz, J. V.; Cui, Q.; Baboul, A. G.; Clifford, S.; Cioslowski, J.; Stefanov, B. B.; Liu, G.; Liashenko, A.; Piskorz, P.; Komaromi, I.; Martin, R. L.; Fox, D. J.; Keith, T.; Al-Laham, M. A.; Peng, C. Y.; Nanayakkara, A.; Challacombe, M.; Gill, P. M. W.; Johnson, B.; Chen, W.; Wong, M. W.; Gonzalez, C.; Pople, J. A. Gaussian 03, Revision C.02; Gaussian, Inc.: Wallingford, CT, 2004.

(27) Dunning, T. H. *J. Phys. Chem. A* **2000**, *104*, 9062.

(28) Shavitt, I. *Isr. J. Chem.* **1993**, *33*, 357.

(29) Eckart, C. *Phys. Rev.* **1935**, *47*, 552.

(30) Louck, J. D.; Galbraith, H. W. *Rev. Mod. Phys.* **1976**, *48*, 69.

(31) Bačić, Z.; Light, J. C. *Annu. Rev. Phys. Chem.* **1989**, *40*, 469.

(32) Wei, H.; Carrington, T. *J. Chem. Phys.* **1992**, *97*, 3029.

(33) Echave, J.; Clary, D. C. *Chem. Phys. Lett.* **1992**, *190*, 225.

(34) Shimanouchi, T. Molecular Vibrational Frequencies. In *NIST Chemistry WebBook, NIST Standard Reference Database*; Mallard, W. G., Linstrom, P. J., Eds.; National Institute of Standards and Technology: Gaithersburg, MD, 2005; Vol. 69 (http://webbook.nist.gov).

(35) Herzberg, G. *Molecular Spectra and Molecular Structure II. Infrared and Raman Spectra of Polyatomic Molecules*; Van Nostrand Reinhold Company Inc.: New York, 1945; Vol. II.

(36) Glendening, E. D.; Reed, A. E.; Carpenter, J. E.; Weinhold, F. *NBO* Version 3.1.

(37) Carpenter, J. E.; Weinhold, F. *J. Mol. Struct. THEOCHEM* **1988**, *169*, 41.

(38) Foster, J. P.; Weinhold, F. *J. Am. Chem. Soc.* **1980**, *102*, 7211.

(39) Pople, J. A.; Scott, A. P.; Wong, M. W.; Radom, L. *Isr. J. Chem.* **1993**, *33*, 345.

(40) Fast, P. L.; Corchado, J.; Sanchez, M. L.; Truhlar, D. G. *J. Phys. Chem. A* **1999**, *103*, 3139.

(41) Zhao, Y.; Lynch, B. J.; Truhlar, D. G. *J. Phys. Chem. A* **2004**, *108*, 4786.

(42) Horvath, S.; McCoy, A. B.; Elliott, B. M.; Weddle, G. H.; Roscioli, J. R.; Johnson, M. A. In preparation.

(43) Kurnig, I. J.; Scheiner, S. *Int. J. Quantum Chem., Quantum Biol. Symp.* **1987**, *14*, 47.

(44) Hunt, S. W.; Higgins, K. J.; Craddock, M. B.; Brauer, C. S.; Leopold, K. R. *J. Am. Chem. Soc.* **2003**, *125*, 13850.

JP805616M